CMS PAPER SMP-20-001

DRAFT
CMS Paper

The content of this note is intended for CMS internal use and distribution only

2020/02/02
Archive Hash: 157c00d
Archive Date: 2020/02/02

Search for vector boson scattering and constraints on anomalous quartic couplings in events with four leptons and two jets in proton-proton collisions at $\sqrt{s} = 13$ TeV

The CMS Collaboration

Abstract

A search for the electroweak production of two jets in association with two Z bosons and constraints on anomalous quartic gauge couplings are presented. The analysis is based on a data sample of proton-proton collisions at $\sqrt{s} = 13$ TeV collected with the CMS detector in 2016, 2017 and 2018, and corresponding to an integrated luminosity of 137.1 fb^{-1}. The search is performed in the fully leptonic final state $\text{ZZ} \rightarrow \ell\ell\ell'\ell'$, where $\ell, \ell' = \text{e}, \mu$. The electroweak production of two Z bosons in association with two jets is measured with an observed (expected) significance of XXX (3.3) standard deviations . Fiducial cross sections for the electroweak production is measured to be $\sigma_{\text{EW}}(pp \rightarrow \text{ZZ}jj \rightarrow \ell\ell\ell'\ell' jj) = XXX^{+X}_{-X}(\text{stat})^{+X}_{-X}(\text{syst})$ fb, in agreement with the standard model prediction. Limits on anomalous quartic gauge couplings are derived in terms of the effective field theory operators T0, T1, T2, T8 and T9.

1 Introduction

In the standard model (SM) the electroweak (EW) vector bosons, like the other fundamental particles, acquire their masses through the coupling to the Higgs field. While the photon remains massless, with only two degrees of freedom of polarization (transverse), the W and Z bosons, together with the mass, acquire an additional degree of freedom (longitudinal), breaking the electroweak symmetry (EWSB). Thus, the scattering of massive vector bosons is at the heart of the EWSB mechanism and its study can lead to significant insight into the origin of particle masses.

At the Large Hadron Collider (LHC), the vector boson scattering (VBS) is the interaction of two electroweak vector bosons emitted by quarks q from the two colliding protons. The scattering involves triple and quartic gauge couplings as predicted in the SM. The VBS channel is generally labeled by the type of outgoing vector bosons. In association with the outgoing EW bosons, two jets coming from the scattered quarks are emitted in the forward-backward region of the detector, giving rise to the so-called rapidity gap [1, 2], where no hadronic activity is foreseen at tree level. The decay of the vector bosons into fermions f defines the final signature of the VBS-like event. The pure VBS contributions, however, are embedded into a wider set of possible processes 2f $\to$ 6f, with which they interfere. While all processes at the order α_{EW}^6, at tree level, shall be considered together, the processes at the order $\alpha_{\mathrm{EW}}^4\alpha_{\mathrm{QCD}}^2$ where at tree level the jets are induced by quantum chromodynamics (QCD), can be factorized out and accounted separately as background (refered to as QCD-induced background). Among the processes of the first type there are also contributions where none, only one, or three fermion pairs come from a vector boson decay. Although with specific cuts on the di-fermion invariant masses those events can be considerably reduced, they cannot be totally suppressed. Therefore, all events 2f $\to$ 6f at $O(\alpha_{\mathrm{EW}}^6)$ that satisfy the signal selection are considered in this analysis as signal.

Both the ATLAS and CMS Collaborations have performed searches for the EW production of jets in association with massive vector bosons, using data from pp collisions at the center-of-mass energy of 13 TeV. The ATLAS Collaboration observed both the EW production of two jets in association with a same-sign W boson pair [3] and of a $\mathrm{W}^{\pm}\mathrm{Z}$ boson pair [4], in the fully leptonic decay channel, and measured the EW diboson production (WW, WZ, ZZ) in association with a high-mass dijet system in semileptonic final states [5], with an observed significance of 2.7 standard deviations (s.d.). The CMS Collaboration observed the formation of two EW-induced jets contemporary with the production of two same-sign W's [6] and measured the EW production of jets in association with WZ [7] and ZZ [8], with an observed significance of 2.2 and 2.7 s.d., respectively.

This paper presents the measurement of the EW production of two jets in association with two Z bosons in the fully leptonic final state, where both Z bosons decay into electrons or muons, $ZZ \to \ell\ell\ell'\ell'$ ($\ell, \ell' = \mathrm{e}, \mu$). Despite a low cross section, a small $\mathrm{Z} \to \ell\ell$ branching fraction, and a large QCD-induced background, this channel provides a clean leptonic final state resulting in a small instrumental background, where one or more of the reconstructed lepton candidates originate from the misidentification of jet fragments or from non-prompt leptons.

The search for the EW-induced production of the $\ell\ell\ell'\ell'$jj final state is carried out using pp collisions at $\sqrt{s} = 13\,\mathrm{TeV}$ recorded with the CMS detector at the LHC. The data set corresponds to an integrated luminosity of $137.1\,\mathrm{fb}^{-1}$ collected in 2016, 2017, and 2018. A discriminant based on a matrix element likelihood approach (MELA) [9–13] is used to extract the signal significance and to measure the cross sections for the EW and the EW+QCD ZZ+jets production in a fiducial volume. Finally, the selected $\ell\ell\ell'\ell'$jj events are used to constrain anomalous quartic gauge couplings (aQGC) described in the effective field theory approach [14] by the operators

T0, T1, and T2 as well as the neutral-current operators T8 and T9 [15].

2 The CMS detector

The central feature of the CMS apparatus is a superconducting solenoid of 6 m internal diameter, providing a magnetic field of 3.8 T. Within the solenoid volume are a silicon pixel and strip tracker, a lead tungstate crystal electromagnetic calorimeter (ECAL), and a brass and scintillator hadron calorimeter (HCAL), each composed of a barrel and two endcap sections. An entirely new pixel detector has been installed in 2017, featuring a full silicon device with 4 layers in the barrel and 3 disks in the endcaps [16], providing a four hits coverage system and reduced material budget in front of the calorimeters. Forward calorimeters extend the pseudorapidity (η) coverage provided by the barrel and endcap detectors. Muons are measured in gas-ionization detectors embedded in the steel flux-return yoke outside the solenoid. A more detailed description of the CMS detector, together with a definition of the coordinate system used and the relevant kinematic variables, can be found in Ref. [17].

3 Signal and background simulation

Several Monte Carlo event generators are used to simulate the signal and background contributions. The simulated samples are employed to optimize the event selection, evaluate the signal efficiency and acceptance, and to model the signal and irreducible background distributions in the signal extraction fit.

The EW production of two Z bosons and two final-state quarks, where the Z bosons decay leptonically, is simulated at LO using MADGRAPH5_aMC@NLO v2.4.6 (abbreviated as MG5_aMC in the following) [18]. The leptonic Z boson decays are simulated using MADSPIN [19]. The sample includes triboson processes, where the Z boson pair is accompanied by a third vector boson that decays hadronically, as well as diagrams involving the quartic coupling vertex. The predictions from this sample are cross-checked with those obtained from the LO generator PHANTOM v1.2.8 [20], and excellent agreement in the yields and the distribution exploited for the signal extraction is found.

The leading QCD-induced production of two Z bosons in association with jets, whose contribution with 2 jets in the final state is referred to as $q\overline{q} \rightarrow$ ZZjj QCD, is simulated at next-to-leading order (NLO) with MG5_aMC with up to two extra partons emissions, and merged using the FxFx scheme [21]. Since the samples are produced at NLO, NNLO/NLO K-factors are applied, differentially as a function of m_{ZZ} [22]. Additional NLO EW corrections are applied for $m_{ZZ} > 2m_Z$, following the calculations from Ref. [23]. The interference between the EW and QCD diagrams is evaluated using dedicated samples produced with MG5_aMC at LO. It is found to contribute less than 1% of the total yield and is therefore neglected. The loop-induced production of two Z bosons, whose contribution with 2 jets in the final state is referred to as $gg \rightarrow$ ZZjj QCD, is simulated at LO with 1 extra parton emission using MG5_aMC by explicitly requiring a loop-induced process. An NLO/LO K-factor of 1.3 is applied, extracted from Refs. [24, 25]. A dedicated MG5_aMC simulation of the loop-induced $gg \rightarrow$ ZZjj QCD process is also used to check the modeling of the ZZjj phase space in the MG5_aMC sample, and good agreement is found.

Samples for $t\bar{t}$Z and WWZ production, background processes that contain four prompt, isolated leptons and additional jets in the final state, are simulated with MG5_aMC at NLO.

The simulation of the aQGC processes is performed at LO using MG5_aMC and employs matrix element reweighting to obtain a finely spaced grid in each of the five anomalous couplings probed by the analysis.

The PYTHIA 8 [26, 27] package is used for parton showering, hadronization and the underlying event simulation, with parameters set by the CUETP8M1 tune [28] (2016 data taking period) and the CP5 tune [29] (2017 and 2018 data taking periods). The NNPDF3.0 (NNPDF3.1) set of parton distribution functions (PDFs) [30] is used for the 2016 (2017 and 2018) data taking period. Unless specified otherwise the simulated samples are normalized to the cross sections obtained from the respective event generator.

The detector response is simulated using a detailed description of the CMS detector implemented in the GEANT4 package [31, 32]. The simulated events are reconstructed using the same algorithms as used for the data. The simulated samples include additional interactions in the same and neighboring bunch crossings, referred to as pileup. Simulated events are weighted so that the pileup distribution reproduces that observed in the data, which has an average of about 23 (32) interactions per bunch crossing in 2016 (2017 and 2018).

4 Event reconstruction and selection

The final state should consist of at least two pairs of oppositely charged isolated leptons and at least two hadronic jets. The ZZ selection is similar to that used in the CMS $\mathrm{H} \to \mathrm{ZZ} \to \ell\ell\ell'\ell'$ measurement [33].

The primary triggers require the presence of a pair of loosely isolated leptons, whose exact requirements depend on the data taking year. Triggers requiring a triplet of low-p_{T} leptons, as well as isolated single-electron and single-muon triggers, help to recover efficiency. The overall trigger efficiency for events that satisfy the ZZ selection described below is greater than 98%.

Events are reconstructed using a particle-flow algorithm [34] that reconstructs and identifies each individual particle with an optimized combination of all subdetector information. The reconstructed vertex with the largest value of summed physics-object p_{T}^2 is taken to be the primary pp interaction vertex.

Electrons are identified using a multivariate classifier, which includes observables sensitive to bremsstrahlung along the electron trajectory, the geometrical and energy-momentum compatibility between the electron track and the associated energy cluster in the ECAL, the shape of the electromagnetic shower, and variables that discriminate against electrons originating from photon conversions [35]. The charged, neutral hadrons and photon components of the isolation variable described below are also included as input variables in the electron mutlivariate classifier.

Muons are reconstructed by combining information from the silicon tracker and the muon system [36]. The matching between the inner and outer tracks proceeds either outside-in, starting from a track in the muon system, or inside-out, starting from a track in the silicon tracker. The muons are selected from the reconstructed muon track candidates by applying minimal requirements on the track in both the muon system and silicon tracker, and taking into account compatibility with small energy deposits in the calorimeters.

In order to further suppress electrons from photon conversions and muons originating from in-flight decays of hadrons, for the three-dimensional impact parameter of each lepton track, computed with respect to the primary vertex position, it is required to be less than four times the uncertainty on the impact parameter.

Leptons are required to be isolated from other particles in the event. The relative isolation is defined as

$$R_{\text{iso}} = \Big[\sum_{\substack{\text{charged} \\ \text{hadrons}}} p_{\text{T}} + \max\big(0, \sum_{\substack{\text{neutral} \\ \text{hadrons}}} p_{\text{T}} + \sum_{\text{photons}} p_{\text{T}} - p_{\text{T}}^{\text{PU}}\big)\Big] \Big/ p_{\text{T}}^{\ell}, \tag{1}$$

where the sums run over the charged, neutral hadrons and photons, in a cone defined by $\Delta R \equiv \sqrt{(\Delta\eta)^2 + (\Delta\phi)^2} = 0.3$ around the lepton trajectory. To minimize the contribution of charged particles from pileup to the isolation calculation, charged hadrons are included only if they originate from the primary vertex. The contribution of neutral particles from pileup is p_{T}^{PU}. Leptons with $R_{\text{iso}} < 0.35$ are considered isolated.

The efficiency of the lepton reconstruction and selection is measured in bins of p_{T}^{ℓ} and η^{ℓ} using the tag-and-probe technique. The measured efficiencies are used to correct the simulation. The lepton momentum scales are calibrated in bins of p_{T}^{ℓ} and η^{ℓ} using the J/ψ meson and Z boson leptonic decays.

Jets are reconstructed from particle-flow candidates using the anti-k_{T} clustering algorithm [37], as implemented in the FASTJET package [38], with a distance parameter of 0.4. In order to ensure a good reconstruction efficiency and to reduce the instrumental background as well as the contamination from pileup, loose identification criteria based on the multiplicities and energy fractions carried by charged and neutral hadrons are imposed on jets [39]. Only jets with $|\eta| < 4.7$ are considered.

Jet energy corrections are extracted from data and simulated events to account for the effects of pileup, uniformity of the detector response, and residual differences between the jet energy scale in the data and in the simulation. The jet energy scale calibration [40–42] relies on corrections parameterized in terms of the uncorrected p_{T} and η of the jet, and is applied as a multiplicative factor, scaling the four-momentum vector of each jet. In order to ensure that jets are well measured and to reduce the pileup contamination, all jets must have a corrected p_{T} larger than 30 GeV. Jets from pileup are further rejected using pileup jet identification criteria based on the compatibility of associated track with the primary vertex inside the tracker acceptance and on the topology of the jet shape in the forward region.

A signal event must contain at least two Z candidates, each formed from pairs of isolated electrons or muons of opposite charges. Only reconstructed electrons (muons) with a $p_{\text{T}} >$ 7 (5) GeV are considered. Among the four leptons, the highest p_{T} lepton must have $p_{\text{T}} >$ 20 GeV, and the second-highest p_{T} lepton must have $p_{\text{T}} >$ 12 (10) GeV if it is an electron (muon). All leptons are required to be separated by $\Delta R\,(\ell_1, \ell_2) > 0.02$, and electrons are required to be separated from muons by $\Delta R\,(\text{e}, \mu) > 0.05$.

Within each event, all permutations of leptons giving a valid pair of Z candidates are considered. For each ZZ candidate, the lepton pair with the invariant mass closest to the nominal Z boson mass is denoted Z_1 The other dilepton candidate is denoted Z_2. Both m_{Z_1} and m_{Z_2} are required to have a mass greater than 60 GeV and less than 120 GeV. All pairs of oppositely charged leptons that can be built from the ZZ candidate, regardless of flavor, are required to satisfy $m_{\ell\ell'} > 4$ GeV to suppress backgrounds from hadron decays. If multiple ZZ candidates in an event pass this selection, the one with the largest scalar sum of the Z_2 leptons p_{T} is retained. Finally, the invariant mass of the ZZ system is required to satisfy $m_{\text{ZZ}} > 180$ GeV. This selection is referred to as the ZZ selection.

The search for the EW production of two Z bosons is performed on a subset of events that pass the ZZ selection, namely those that feature at least two jets. The jets are required to be separated from the leptons of the ZZ candidate by $\Delta R > 0.4$. The two highest p_{T} jets are referred to as the tagging jets and their invariant mass is required to be larger than 100 GeV. This selection is referred to as the ZZjj inclusive selection and is used to measure the signal significance, the total fiducial cross-sections and to perform the aQGC search. Additionnaly, two VBS signal-enriched signal sub-regions are defined. A loose VBS signal-enriched region that requires $m_{\mathrm{jj}} > 400\,\mathrm{GeV}$ and $|\Delta\eta_{\mathrm{jj}}| > 2.4$ and corresponds to a signal purity of $\approx$50%, and a tight VBS signal-enriched region that requires $m_{\mathrm{jj}} > 400\,\mathrm{GeV}$ and $|\Delta\eta_{\mathrm{jj}}| > 5$ and corresponds to a signal purity of $\approx$80%. Finally, a background control region is defined from events that satisfy the ZZjj inclusive selection but fail at least one of the criteria that define the loose VBS signal-enriched region.

5 Background estimation

The dominant background arises from the QCD-induced production of two Z bosons in association with jets. The yield and shape of the matrix element discriminant for this irreducible background are taken from simulation, but ultimately constrained by the data in the fit that extracts the EW signal, as described in Section 7. Other irreducible backgrounds arise from processes that produce four genuine high-p_{T} isolated leptons, $\mathrm{pp} \to \mathrm{t\bar{t}Z} + \mathrm{jets}$ and $\mathrm{pp} \to \mathrm{WWZ} + \mathrm{jets}$. These small contributions feature kinematic distributions similar to that of the dominant background and are estimated using simulation.

Reducible backgrounds arise from processes in which heavy-flavor jets produce secondary leptons or from processes in which jets are misidentified as leptons. The lepton identification and isolation requirements significantly suppress this background, which after the selection is very small in the signal region.

The reducible background, referred to as Z + X, is predominately composed of Z + jets events, with minor contributions from $\mathrm{t\bar{t}}$ + jets and WZ + jets processes. This reducible contribution is estimated from data by weighting events from a control region by a lepton misidentification rate which is also determined from data. Events in the control region satisfy the ZZjj inclusive selection, with the exception that the Z_2 is composed from same flavor leptons of the same charge (SS-SF). The SS-SF leptons are requested to pass the three-dimensional impact parameter cut, while no identification nor isolation requirement is imposed.

The lepton misidentification rate is measured by selecting events that feature one Z boson candidate and a third reconstructed lepton. The fraction of events for which the third lepton satisfies the identification and isolation criteria is taken as the lepton misidentification rate. The fake ratios are evaluated using the tight requirement $|m_{\mathrm{Z}_1} - m_{\mathrm{Z}}| < 7\,\mathrm{GeV}$ to reduce the contribution from asymmetric photon conversions, and $p_{\mathrm{T}}^{\mathrm{miss}} < 25\,\mathrm{GeV}$ to suppress the WZ contribution. The procedure is identical to that used in Ref. [33].

6 Systematic uncertainties

Several sources of systematic uncertainties are considered and evaluated by varying each relevant parameter. The resulting changes to the distribution of the matrix element discriminant, both in shape and yield, are taken into account. The uncertainties from the QCD scales for the signal and in jet energy scale are the dominant systematic uncertainties in the measurement. The impact of the variation for each source of uncertainty is summarized below.

Renormalization and factorization scale uncertainties are evaluated by varying both scales independently by factors of two and one-half. It ranges from xx–yy% (4–11%) for the $\mathrm{q\bar{q}} \to \mathrm{ZZjj}$

QCD background (EW signal), depending on the matrix-element discriminant value. For the gg $\rightarrow$ ZZjj QCD, the variations are found to be independent of the matrix-element discriminant value. Since the uncertainty relates to missing higher order corrections that are corrected for using a K-factor, an uncertainty in the normalization of 11% is used for this process, derived from Refs. [24, 25]. The PDF + α_s variations are evaluated following the PDF4LHC prescription [43], and is 3.2% (6.6%) for the $q\overline{q} \rightarrow$ ZZjj QCD background (EW signal). While the PDFs used are different in the different years (see Section 3) the associated uncertainties are found to be very similar. Given the small dependence on the discriminant value a constant value is used for these uncertainties.

The impact of the jet energy scale uncertainty amounts to 4.9% (0.7%) for the $q\overline{q} \rightarrow$ ZZjj QCD background (EW signal) and the impact of the jet energy resolution uncertainty is 2.4% (0.2%) [41, 42]. The uncertainty in the trigger as well as lepton reconstruction and selection efficiency ranges from 2.5% to 9% depending on the final state. The uncertainty in the integrated luminosity is 2.3–2.5% depending on the data taking period [44]. The uncertainty in the data-driven estimate of the reducible background ranges from 33% to 45% depending on the final state. It takes into account the limited number of events in the control regions as well as differences in background composition between the control regions used to determine the lepton misidentification rates and those used to estimate the yield in the signal region.

7 Search for the EW production of ZZ with two jets

After the ZZjj inclusive selection, the expected signal purity is about 6%, with 85% of events coming from QCD-induced production. Additional kinematic selections are therefore necessary to enhance the contribution from EW production. Table 1 presents the expected and observed event yields for the ZZjj inclusive selection as well as for the loose VBS signal-enriched selection that requires $m_{jj} > 400\,\mathrm{GeV}$ and $|\Delta\eta_{jj}| > 2.4$.

Table 1: Signal and background yields for the baseline selection and for the loose VBS signal-enriched selection that requires $m_{jj} > 400\,\mathrm{GeV}$ and $|\Delta\eta_{jj}| > 2.4$.

Year	Signal (ZZjj EW)	Z+X	$q\overline{q} \rightarrow$ ZZjj QCD	gg $\rightarrow$ ZZjj QCD	$t\bar{t}$ +WWZ	Data
			ZZjj inclusive			
2016	5.6 ± 0.6	1.5 ± 0.6	61.4 ± 5.6	19.8 ± 2.7	6.3 ± 0.9	100
2017	6.1 ± 0.7	1.3 ± 0.5	67.9 ± 6.2	22.8 ± 3.1	8.1 ± 1.2	
2018	9.5 ± 1.1	2.5 ± 0.9	98.2 ± 9.0	32.9 ± 4.5	11.9 ± 1.7	
all	21.1 ± 2.3	5.3 ± 2.0	227.4 ± 20.8	75.5 ± 10.3	26.3 ± 3.8	
			VBS signal-enriched (loose)			
2016	4.0 ± 0.4	0.2 ± 0.1	8.6 ± 0.8	4.6 ± 0.6	0.8 ± 0.1	19
2017	4.6 ± 0.5	0.3 ± 0.1	10.1 ± 0.9	5.4 ± 0.7	1.0 ± 0.1	
2018	6.3 ± 0.7	0.4 ± 0.2	16.5 ± 1.5	7.7 ± 1.1	1.7 ± 0.2	
all	14.9 ± 1.7	0.9 ± 0.3	35.2 ± 3.2	17.7 ± 2.4	3.4 ± 0.5	

The determination of the signal strength for the EW production, i.e., the ratio of the measured cross section to the SM expectation $\mu = \sigma/\sigma_{\mathrm{SM}}$, employs a matrix-element discriminant to optimally separate the signal and the QCD background. The discriminant is constructed following the approach described in Ref. [10–12]. The performance of the discriminant are checked against a multivariate discriminant based on a boosted decision tree that includes up to 28 input variables.

Figure 1 (left and center) presents m_{jj} and $|\Delta\eta_{\mathrm{jj}}|$ distributions which are used to define VBS signal-enriched and control regions in the analysis, while the determination of the EW significance and cross-section is performed using all available events.

The distribution of the matrix-element discriminant in the control region defined by selecting events with $m_{\mathrm{jj}} < 400\,\mathrm{GeV}$ or $|\Delta\eta_{\mathrm{jj}}| < 2.4$. Good agreement is observed between the data and SM expectation.

The matrix-element distribution of the matrix-element discriminant for all events in the ZZjj inclusive selection is shown in Fig. 1 (right). The high signal purity contribution is visible at large discriminant values.

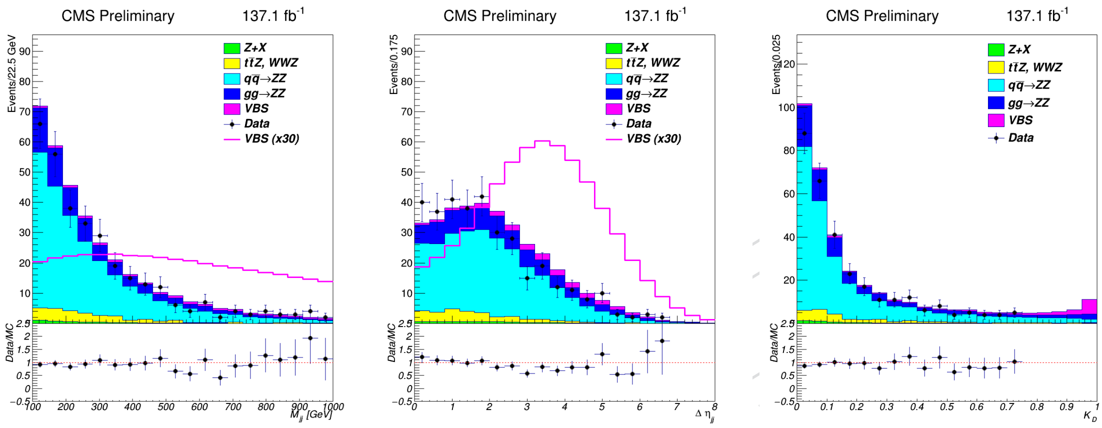

Figure 1: Distribution of m_{jj} (left), $|\Delta\eta_{\mathrm{jj}}|$ (center), and the matrix-element discriminant (right) and for events satisfying the ZZjj inclusive selection. Points represent the data, filled histograms the expected signal and background contributions.

The matrix-element discriminant distribution for events in the ZZjj inclusive selection is used to extract the significance of the EW signal via a maximum-likelihood fit. The expected distributions for the signal and the irreducible backgrounds are taken from the simulation while the reducible background is estimated from the data. The shape and normalization of each distribution are allowed to vary in the fit within the respective uncertainties. This approach constrains the yield of the QCD-induced production from the background-enriched region of the discriminant distribution.

The systematic uncertainties are treated as nuisance parameters in the fit and profiled [45]. The post-fit values are then used to extract the signal strength. The signal strength is measured to be $\mu = xx^{+0.yy}_{-0.zz}\,(\mathrm{stat})\,^{+0.yy}_{-0.zz}\,(\mathrm{syst}) = xx^{+0.yy}_{-0.zz}$ and the background-only hypothesis is excluded with a significance of xx standard deviations (3.3 standard deviations expected).

The measured signal strength is used to determine fiducial cross sections for the EW production and for the EW+QCD production. The fiducial volume is almost identical to the selections imposed at the reconstruction level, and is detailed in Table 2.

The generator-level lepton momenta are corrected by adding the momenta of generator-level photons within $\Delta R(\ell, \gamma) < 0.1$. The kinematic selection of the Z bosons and the final ZZjj candidate proceeds as the reconstruction-level selection.

Table 3 reports the SM cross-sections in the fiducial regions, the fitted value of the signal

Table 2: Particle-level selections used to define the fiducial regions for EWK and EWK+QCD cross-sections.

Object	Selection
	ZZjj baseline
Leptons	$p_T(\ell_1) > 20$ GeV
	$p_T(\ell_2) > 10$ GeV
	$p_T(\ell) > 5$ GeV
	$\lvert\eta(\ell)\rvert < 2.5$
	(γ with $\Delta R(\ell, \gamma) < 0.1$ added to ℓ 4-vector)
Z and ZZ	$60 < m(\ell\ell) < 120$ GeV
	$m(4\ell) > 180$ GeV
Jets	at least 2
	$p_T(j) > 30$ GeV
	$\lvert\eta(j)\rvert < 4.7$
	$m_{jj} > 100$ GeV
	$\Delta R(\ell, j) > 0.4$ for each ℓ, j
	VBS-enriched (loose)
	ZZjj baseline +
Jets	$\Delta\eta(jj) > 2.4$
	$m_{jj} > 400$ GeV
	VBS-enriched (tight)
	ZZjj baseline +
Jets	$\Delta\eta(jj) > 5$
	$m_{jj} > 400$ GeV

strength μ with its statistical and systematic uncertainty and the resulting measured cross-sections.

Table 3: SM cross-sections in the fiducial regions, the fitted value of the signal strength μ with its total uncertainty (statistical only in parenthesis) and the resulting measured cross-sections.

	SM σ (fb)	μ_{exp}	μ_{obs}	Measured σ (fb)
		ZZjj baseline		
EW	0.275 ± 0.021	$1.00\,^{+0.44}_{-0.37}\,(^{+0.40}_{-0.35})$		
EW+QCD	5.35 ± 0.21	$1.00\,^{+0.11}_{-0.10}\,(\pm\,0.06)$		
		VBS signal-enriched (loose)		
EW	0.186 ± 0.015	$1.00\,^{+0.46}_{-0.38}\,(^{+0.41}_{-0.36})$		
EW+QCD	1.21 ± 0.05	$1.00\,^{+0.14}_{-0.15}\,(^{+0.12}_{-0.13})$		
		VBS signal-enriched (tight)		
EW	$xx \pm$ yy	$xx\,^{+0.yy}_{-0.yy}\,(^{+0.yy}_{-0.yy})$		
EW+QCD	$xx \pm$ yy	$1.00\,^{+0.yy}_{-0.yy}\,(^{+0.yy}_{-0.yy})$		

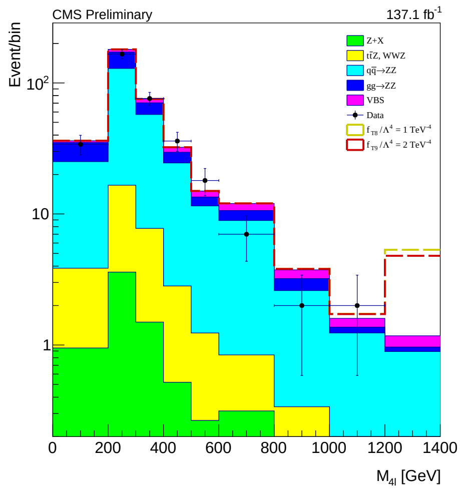

Figure 2: ZZ invariant mass distribution in the ZZjj inclusive selection together with the SM prediction and two hypotheses for the aQGC coupling strengths. Points represent the data, filled histograms the expected signal and background contributions. The last bin includes all contributions with $m_{ZZ} > 1200\,\text{GeV}$.

Table 4: Expected and observed lower and upper 95% CL limits on the couplings of the quartic operators T0, T1, and T2, as well as the neutral current operators T8 and T9. The unitarity bounds are also listed. All coupling parameter limits are in TeV^{-4}, while the unitarity bounds are in TeV.

Coupling	Exp. lower	Exp. upper	Obs. lower	Obs. upper	Unitarity bound
f_{T0}/Λ^4	-0.53	0.52	xx	xx	xx
f_{T1}/Λ^4	-0.71	0.71	xx	xx	xx
f_{T2}/Λ^4	-1.42	1.39	xx	xx	xx
f_{T8}/Λ^4	-0.99	0.99	xx	xx	xx
f_{T9}/Λ^4	-2.12	2.12	xx	xx	xx

8 Limits on anomalous quartic gauge couplings

The ZZjj channel is particularly sensitive to the operators T0, T1, and T2, as well as the neutral current operators T8 and T9 [15]. The m_{ZZ} distribution is used to constrain the aQGC coupling parameters f_{Ti}/Λ^4. The expected yield enhancement exhibits a quadratic dependence on the anomalous couplings, and a parabolic function is fitted to the per-mass bin yields, allowing for an interpolation between the discrete coupling parameters of the simulated aQGC signals. The statistical analysis employs the same methodology used for the signal strength, including the profiling of the systematic uncertainties. The distributions of the background model, including the EW component, are normalized to their measured values in the EW signal extraction (Sec. 7). The Wald Gaussian approximation and Wilks' theorem are used to derive 95% confidence level (CL) limits on the aQGC parameters [46–48]. The measurement is statistically limited.

Figure 2 shows the expected m_{ZZ} distribution for the SM and two aQGC scenarios. Table 4 lists the individual lower and upper limits obtained by setting all other anomalous couplings to zero, as well as the unitarity bound. The unitarity bound is determined using the VBFNLO framework [49] as the scattering energy m_{ZZ} at which the aQGC coupling strength set equal to the observed limit would result in a scattering amplitude that would violate unitarity.

9 Summary

A search was made for the electroweak production of two jets in association with two Z bosons in the four-lepton final state in proton-proton collisions at 13 TeV. The data correspond to an integrated luminosity of 137 fb^{-1} collected with the CMS detector at the LHC.

The electroweak production of two jets in association with a pair of Z bosons is measured with an observed (expected) significance of XX.X (3.3) standard deviations. The fiducial cross section is measured to be $\sigma_{\text{fid}} = XXX^{+Y}_{-Z}(\text{stat})^{+Y}_{-Z}(\text{syst})$ fb, which is consistent with the standard model prediction.

Limits on anomalous quartic gauge couplings are set at the 95% confidence level in terms of effective field theory operators, with units in TeV^{-4}:

$$
\begin{aligned}
-XXX < f_{T_0}/\Lambda^4 < YYY \\
-XXX < f_{T_1}/\Lambda^4 < YYY \\
-XXX < f_{T_2}/\Lambda^4 < YYY \\
-XXX < f_{T_8}/\Lambda^4 < YYY \\
-XXX < f_{T_9}/\Lambda^4 < YYY
\end{aligned}
$$

Acknowledgments

We congratulate our colleagues in the CERN accelerator departments for the excellent performance of the LHC and thank the technical and administrative staffs at CERN and at other CMS institutes for their contributions to the success of the CMS effort. In addition, we gratefully acknowledge the computing centres and personnel of the Worldwide LHC Computing Grid for delivering so effectively the computing infrastructure essential to our analyses. Finally, we acknowledge the enduring support for the construction and operation of the LHC and the CMS detector provided by the following funding agencies: BMWFW and FWF (Austria); FNRS and FWO (Belgium); CNPq, CAPES, FAPERJ, and FAPESP (Brazil); MES (Bulgaria); CERN; CAS, MoST, and NSFC (China); COLCIENCIAS (Colombia); MSES and CSF (Croatia); RPF (Cyprus); SENESCYT (Ecuador); MoER, ERC IUT, and ERDF (Estonia); Academy of Finland, MEC, and HIP (Finland); CEA and CNRS/IN2P3 (France); BMBF, DFG, and HGF (Germany); GSRT (Greece); OTKA and NIH (Hungary); DAE and DST (India); IPM (Iran); SFI (Ireland); INFN (Italy); MSIP and NRF (Republic of Korea); LAS (Lithuania); MOE and UM (Malaysia); BUAP, CINVESTAV, CONACYT, LNS, SEP, and UASLP-FAI (Mexico); MBIE (New Zealand); PAEC (Pakistan); MSHE and NSC (Poland); FCT (Portugal); JINR (Dubna); MON, RosAtom, RAS, RFBR and RAEP (Russia); MESTD (Serbia); SEIDI, CPAN, PCTI and FEDER (Spain); Swiss Funding Agencies (Switzerland); MST (Taipei); ThEPCenter, IPST, STAR, and NSTDA (Thailand); TUBITAK and TAEK (Turkey); NASU and SFFR (Ukraine); STFC (United Kingdom); DOE and NSF (USA).

Individuals have received support from the Marie-Curie programme and the European Research Council and Horizon 2020 Grant, contract No. 675440 (European Union); the Leventis Foundation; the A. P. Sloan Foundation; the Alexander von Humboldt Foundation; the Belgian Federal Science Policy Office; the Fonds pour la Formation à la Recherche dans l'Industrie et dans l'Agriculture (FRIA-Belgium); the Agentschap voor Innovatie door Wetenschap en Technologie (IWT-Belgium); the Ministry of Education, Youth and Sports (MEYS) of the Czech Republic; the Council of Science and Industrial Research, India; the HOMING PLUS programme of the Foundation for Polish Science, cofinanced from European Union, Regional

Development Fund, the Mobility Plus programme of the Ministry of Science and Higher Education, the National Science Center (Poland), contracts Harmonia 2014/14/M/ST2/00428, Opus 2014/13/B/ST2/02543, 2014/15/B/ST2/03998, and 2015/19/B/ST2/02861, Sonata-bis 2012/07/E/ST2/01406; the National Priorities Research Program by Qatar National Research Fund; the Programa Clarín-COFUND del Principado de Asturias; the Thalis and Aristeia programmes cofinanced by EU-ESF and the Greek NSRF; the Rachadapisek Sompot Fund for Postdoctoral Fellowship, Chulalongkorn University and the Chulalongkorn Academic into Its 2nd Century Project Advancement Project (Thailand); and the Welch Foundation, contract C-1845.

References

[1] D. Rainwater, R. Szalapski, and D. Zeppenfeld, "Probing color singlet exchange in Z+2-jet events at the CERN LHC", *Phys. Rev. D* **54** (1996) 6680, `doi:10.1103/PhysRevD.54.6680`, `arXiv:hep-ph/9605444`.

[2] V. A. Khoze, M. G. Ryskin, W. J. Stirling, and P. H. Williams, "A Z-monitor to calibrate Higgs production via vector boson fusion with rapidity gaps at the LHC", *Eur. Phys. J. C* **26** (2003) 429, `doi:10.1140/epjc/s2002-01069-2`, `arXiv:hep-ph/0207365`.

[3] ATLAS Collaboration, "Observation of electroweak production of a same-sign W boson pair in association with two jets in pp collisions at $\sqrt{s} = 13$ TeV with the ATLAS detector", *Phys. Rev. Lett.* **123** (2019), no. 16, 161801, `doi:10.1103/PhysRevLett.123.161801`, `arXiv:1906.03203`.

[4] ATLAS Collaboration, "Observation of electroweak $W^{\pm}Z$ boson pair production in association with two jets in pp collisions at $\sqrt{s} = 13$ TeV with the ATLAS detector", *Phys. Lett. B* **793** (2019) 469–492, `doi:10.1016/j.physletb.2019.05.012`, `arXiv:1812.09740`.

[5] ATLAS Collaboration, "Search for the electroweak diboson production in association with a high-mass dijet system in semileptonic final states in pp collisions at $\sqrt{s} = 13$ TeV with the ATLAS detector", *Phys. Rev. D* **100** (2019), no. 3, 032007, `doi:10.1103/PhysRevD.100.032007`, `arXiv:1905.07714`.

[6] CMS Collaboration, "Observation of electroweak production of same-sign W boson pairs in the two jet and two same-sign lepton final state in proton-proton collisions at $\sqrt{s} = 13$ TeV", *Phys. Rev. Lett.* **120** (2018), no. 8, 081801, `doi:10.1103/PhysRevLett.120.081801`, `arXiv:1709.05822`.

[7] CMS Collaboration, "Measurement of electroweak WZ boson production and search for new physics in WZ + two jets events in pp collisions at $\sqrt{s} = 13$TeV", *Phys. Lett. B* **795** (2019) 281–307, `doi:10.1016/j.physletb.2019.05.042`, `arXiv:1901.04060`.

[8] CMS Collaboration, "Measurement of vector boson scattering and constraints on anomalous quartic couplings from events with four leptons and two jets in proton-proton collisions at $\sqrt{s} = 13$ TeV", *Phys. Lett.* **B774** (2017) 682–705, `doi:10.1016/j.physletb.2017.10.020`, `arXiv:1708.02812`.

[9] CMS Collaboration, "Observation of a New Boson at a Mass of 125 GeV with the CMS Experiment at the LHC", *Phys. Lett.* **B716** (2012) 30–61, `doi:10.1016/j.physletb.2012.08.021`, `arXiv:1207.7235`.

[10] S. Bolognesi et al., “On the spin and parity of a single-produced resonance at the LHC”, *Phys. Rev. D* **86** (2012) 095031, doi:10.1103/PhysRevD.86.095031, arXiv:1208.4018.

[11] Y. Gao et al., “Spin determination of single-produced resonances at hadron colliders”, *Phys. Rev. D* **81** (2010) 075022, doi:10.1103/PhysRevD.81.075022, arXiv:1001.3396. [Erratum: doi:10.1103/PhysRevD.81.079905].

[12] I. Anderson et al., “Constraining anomalous HVV interactions at proton and lepton colliders”, *Phys. Rev. D* **89** (2014) 035007, doi:10.1103/PhysRevD.89.035007, arXiv:1309.4819.

[13] A. V. Gritsan, R. Rntsch, M. Schulze, and M. Xiao, “Constraining anomalous Higgs boson couplings to the heavy flavor fermions using matrix element techniques”, *Phys. Rev.* **D94** (2016), no. 5, 055023, doi:10.1103/PhysRevD.94.055023, arXiv:1606.03107.

[14] C. Degrande et al., “Effective field theory: A modern approach to anomalous couplings”, *Annals Phys.* **335** (2013) 21, doi:10.1016/j.aop.2013.04.016, arXiv:1205.4231.

[15] O. J. P. Éboli, M. C. Gonzalez-Garcia, and J. K. Mizukoshi, “$pp \to jj e^{\pm}\mu^{\pm}\nu\nu$ and $jj e^{\pm}\mu^{\mp}\nu\nu$ at $\mathcal{O}(\alpha_{\rm em}^6)$ and $\mathcal{O}(\alpha_{\rm em}^4\alpha_s^2)$ for the study of the quartic electroweak gauge boson vertex at CERN LHC”, *Phys. Rev. D* **74** (2006) 073005, doi:10.1103/PhysRevD.74.073005, arXiv:hep-ph/0606118.

[16] A. Dominguez et al., “CMS Technical Design Report for the Pixel Detector Upgrade”, Technical Report CERN-LHCC-2012-016. CMS-TDR-11, Sep, 2012. doi:10.2172/1151650.

[17] CMS Collaboration, “The CMS experiment at the CERN LHC”, *JINST* **3** (2008) S08004, doi:10.1088/1748-0221/3/08/S08004.

[18] J. Alwall et al., “The automated computation of tree-level and next-to-leading order differential cross sections, and their matching to parton shower simulations”, *JHEP* **07** (2014) 079, doi:10.1007/JHEP07(2014)079, arXiv:1405.0301.

[19] P. Artoisenet, R. Frederix, O. Mattelaer, and R. Rietkerk, “Automatic spin-entangled decays of heavy resonances in Monte Carlo simulations”, *JHEP* **03** (2013) 015, doi:10.1007/JHEP03(2013)015, arXiv:1212.3460.

[20] A. Ballestrero et al., “PHANTOM: A Monte Carlo event generator for six parton final states at high energy colliders”, *Comput. Phys. Commun.* **180** (2009) 401, doi:10.1016/j.cpc.2008.10.005, arXiv:0801.3359.

[21] R. Frederix and S. Frixione, “Merging meets matching in MC@NLO”, *JHEP* **12** (2012) 061, doi:10.1007/JHEP12(2012)061, arXiv:1209.6215.

[22] M. Grazzini, S. Kallweit, and D. Rathlev, “ZZ production at the LHC: Fiducial cross sections and distributions in NNLO QCD”, *Phys. Lett. B* **750** (2015) 407, doi:http://dx.doi.org/10.1016/j.physletb.2015.09.055, arXiv:1507.06257.

[23] S. Gieseke, T. Kasprzik, and J. H. Kuehn, “Vector-boson pair production and electroweak corrections in HERWIG++”, *Eur. Phys. J.* **C74** (2014), no. 8, 2988, doi:10.1140/epjc/s10052-014-2988-y, arXiv:1401.3964.

[24] F. Caola, K. Melnikov, R. Rntsch, and L. Tancredi, "QCD corrections to ZZ production in gluon fusion at the LHC", *Phys. Rev.* **D92** (2015), no. 9, 094028, doi:10.1103/PhysRevD.92.094028, arXiv:1509.06734.

[25] F. Caola et al., "QCD corrections to vector boson pair production in gluon fusion including interference effects with off-shell Higgs at the LHC", *JHEP* **07** (2016) 087, doi:10.1007/JHEP07(2016)087, arXiv:1605.04610.

[26] T. Sjöstrand, S. Mrenna, and P. Skands, "PYTHIA 6.4 physics and manual", *JHEP* **05** (2006) 026, doi:10.1088/1126-6708/2006/05/026, arXiv:hep-ph/0603175.

[27] T. Sjöstrand et al., "An introduction to PYTHIA 8.2", *Comput. Phys. Commun.* **191** (2015) 159, doi:10.1016/j.cpc.2015.01.024, arXiv:1410.3012.

[28] CMS Collaboration, "Event generator tunes obtained from underlying event and multiparton scattering measurements", *Eur. Phys. J. C* **76** (2016) 155, doi:10.1140/epjc/s10052-016-3988-x, arXiv:1512.00815.

[29] CMS Collaboration, "Extraction and valiudation of a new set of cms pythia8 tunes from unerlying-event measurements", *Submitted to Eur. Phys. J. C* arXiv:1903.12179.

[30] NNPDF Collaboration, "Parton distributions for the LHC run II", *JHEP* **04** (2015) 040, doi:10.1007/JHEP04(2015)040, arXiv:1410.8849.

[31] GEANT4 Collaboration, "GEANT4—a simulation toolkit", *Nucl. Instrum. Meth. A* **506** (2003) 250, doi:10.1016/S0168-9002(03)01368-8.

[32] J. Allison et al., "GEANT4 developments and applications", *IEEE Trans. Nucl. Sci.* **53** (2006) 270, doi:10.1109/TNS.2006.869826.

[33] A. M. Sirunyan et al., "Measurements of properties of the higgs boson decaying into the four-lepton final state in pp collisions at s = 13

$$\sqrt{s} = 13$$

tev", *Journal of High Energy Physics* **2017** (Nov, 2017) doi:10.1007/jhep11(2017)047.

[34] CMS Collaboration, "Particle-flow reconstruction and global event description with the CMS detector", (2017). arXiv:1706.04965. Submitted to JINST.

[35] CMS Collaboration, "Performance of electron reconstruction and selection with the CMS detector in proton-proton collisions at $\sqrt{s} = 8\,\text{TeV}$", *JINST* **10** (2015) P06005, doi:10.1088/1748-0221/10/06/P06005, arXiv:1502.02701.

[36] CMS Collaboration, "Performance of CMS muon reconstruction in pp collision events at $\sqrt{s} = 7\,\text{TeV}$", *JINST* **7** (2012) P10002, doi:10.1088/1748-0221/7/10/P10002, arXiv:1206.4071.

[37] M. Cacciari, G. P. Salam, and G. Soyez, "The anti-k_t jet clustering algorithm", *JHEP* **04** (2008) 063, doi:10.1088/1126-6708/2008/04/063, arXiv:0802.1189.

[38] M. Cacciari, G. P. Salam, and G. Soyez, "FastJet user manual", *Eur. Phys. J. C* **72** (2012) 1896, doi:10.1140/epjc/s10052-012-1896-2, arXiv:1111.6097.

[39] CMS Collaboration, "Jet algorithms performance in 13 TeV data", CMS Physics Analysis Summary CMS-PAS-JME-16-003, 2017.

[40] CMS Collaboration, "Determination of jet energy calibration and transverse momentum resolution in CMS", *JINST* **6** (2011) P11002, doi:10.1088/1748-0221/6/11/P11002, arXiv:1107.4277.

[41] CMS Collaboration, "Jet energy scale and resolution in the CMS experiment in pp collisions at 8 TeV", *JINST* **12** (2017) P02014, doi:10.1088/1748-0221/12/02/P02014, arXiv:1607.03663.

[42] CMS Collaboration, "Jet energy scale and resolution performances with 13 TeV data", CMS Detector Performance Summary CMS-DP-2016-020, 2016.

[43] J. Butterworth et al., "PDF4LHC recommendations for LHC Run II", *J. Phys. G* **43** (2016) 023001, doi:10.1088/0954-3899/43/2/023001, arXiv:1510.03865.

[44] CMS Collaboration, "CMS luminosity measurement for the 2016/2017/2018 data-taking period at $\sqrt{s} = 13$ TeV", technical report.

[45] ATLAS and CMS Collaborations, LHC Higgs Combination Group, "Procedure for the LHC higgs boson search combination in Summer 2011", CMS-NOTE-2011-005; ATL-PHYS-PUB-2011-11, 2011.

[46] A. L. Read, "Presentation of search results: the CL_s technique", *J. Phys. G* **28** (2002) 2693, doi:10.1088/0954-3899/28/10/313.

[47] T. Junk, "Confidence level computation for combining searches with small statistics", *Nucl. Instrum. Meth. A* **434** (1999) 435, doi:10.1016/S0168-9002(99)00498-2, arXiv:hep-ex/9902006.

[48] G. Cowan, K. Cranmer, E. Gross, and O. Vitells, "Asymptotic formulae for likelihood-based tests of new physics", *Eur. Phys. J. C* **71** (2011) 1554, doi:10.1140/epjc/s10052-011-1554-0, arXiv:1007.1727. [Erratum: doi:10.1140/epjc/s10052-013-2501-z].

[49] K. Arnold et al., "VBFNLO: A Parton level Monte Carlo for processes with electroweak bosons", *Comput. Phys. Commun.* **180** (2009) 1661–1670, doi:10.1016/j.cpc.2009.03.006, arXiv:0811.4559.